Original

Sommer, T.; Carpenter, J.R.; Wueest, A.:

Double-diffusive interfaces in Lake Kivu reproduced by direct numerical simulations

In: Geophysical Research Letters (2014) AGU

DOI: 10.1002/2014GL060716

AGU PUBLICATIONS

Geophysical Research Letters

RESEARCH LETTER
10.1002/2014GL060716

Key Points:
- Two-dimensional DNS reproduces interface thicknesses of in situ microstructure profiles
- The heat transport through the interface is molecular for density ratios ≥ 3
- The scaling law used for estimating Arctic heat flux requires correction

Correspondence to:
T. Sommer,
tobias.sommer@eawag.ch

Citation:
Sommer, T., J. R. Carpenter, and A. Wüest (2014), Double-diffusive interfaces in Lake Kivu reproduced by direct numerical simulations, *Geophys. Res. Lett.*, *41*, 5114–5121, doi:10.1002/2014GL060716.

Received 4 JUN 2014
Accepted 11 JUL 2014
Accepted article online 14 JUL 2014
Published online 29 JUL 2014

Double-diffusive interfaces in Lake Kivu reproduced by direct numerical simulations

Tobias Sommer[1,2], Jeffrey R. Carpenter[1,3,4], and Alfred Wüest[1,2,5]

[1]Eawag, Surface Waters-Research and Management, Kastanienbaum, Switzerland, [2]Institute of Biogeochemistry and Pollutant Dynamics, ETH Zurich, Zurich, Switzerland, [3]Department of Geology and Geophysics, Yale University, New Haven, Connecticut, USA, [4]Institute for Coastal Research, Helmholtz-Zentrum Geesthacht, Geesthacht, Germany, [5]Physics of Aquatic Systems Laboratory-Margaretha Kamprad Chair of Environmental Science and Limnology, ENAC, EPFL, Lausanne, Switzerland

Abstract Double diffusion transforms uniform background gradients of temperature and salinity into "staircases" of homogeneous mixed layers that are separated by high-gradient interfaces. Direct numerical simulations (DNS) and microstructure measurements are two independent methods of estimating double-diffusive fluxes. By performing DNS under similar conditions as found in our measurements in Lake Kivu, we are able to compare results from both methods for the first time. We find that (i) the DNS reproduces the measured interface thicknesses of in situ microstructure profiles, (ii) molecular heat fluxes through interfaces capture the total vertical heat fluxes for density ratios larger than three, and (iii) the commonly used heat flux parameterization underestimates the total fluxes by a factor of 1.3 to 2.2.

1. Introduction

The diffusive type of double diffusion occurs in oceans and lakes where both temperature and salinity increase with depth, creating staircase-like structures with nearly homogeneous mixed layers separated by thin high-gradient interfaces [*Schmitt*, 1994; *Kelley et al*., 2003; *Ruddick and Gargett*, 2003]. Estimating the vertical fluxes through such staircases is important, in particular in the Arctic Ocean, where double-diffusive heat transport to the overlying ice needs to be quantified [*Timmermans et al*., 2008; *Turner*, 2010].

With increasing computation power, direct numerical simulations (DNS) are becoming more attractive to study complex fluid behavior such as double diffusion [*Kimura and Smyth*, 2007; *Simeonov and Stern*, 2008; *Noguchi and Niino*, 2010a, 2010b; *Traxler et al*., 2011; *Carpenter et al*., 2012a; *Flanagan et al*., 2013]. However, DNS are still limited by the size and dimensions of the computational domain at sufficient grid resolution and rely on choices of the boundary conditions that may not be representative of natural staircases. Given all the sources of variability and the presence of other processes that may be acting to alter fluxes across interfaces (e.g., mean shear as found in the salt finger interfaces of the Caribbean Sheets and Layers Transects experiment [*Gregg and Sanford*, 1987]), comparing in situ measurements to DNS is an extremely valuable approach for understanding both the ability of DNS to reproduce natural dynamics and signals found in the in situ measurements.

In this work we compare high-resolution microstructure profiles of temperature and conductivity measured in Lake Kivu to two-dimensional DNS. In addition to a qualitative explanation of common interface and mixed layer structures, we compare interface thicknesses and the related molecular fluxes through the interfaces in both systems. The molecular fluxes are then compared to the total vertical fluxes in the DNS and to the commonly applied flux parameterization by *Kelley* [1990] as well as the theories of *Linden and Shirtcliffe* [1978] and *Fernando* [1989a]. Notation and definitions are summarized in Table 1.

2. Methods

2.1. Lake Kivu Data

During two field campaigns to Lake Kivu (East Africa, surface area of 2300 km^2, maximum depth of 485 m, and volume of 550 km^3) [*Descy et al*., 2012] in 2010 and 2011, we measured 225 microstructure profiles of temperature and conductivity with a Vertical Microstructure Profiler (Rockland Scientific International, Canada) covering a total profiling length of ~55 km [*Sommer et al*., 2013b]. Double-diffusive staircases are found below ~100 m depth containing up to 300 interfaces and mixed layers [*Newman*, 1976; *Schmid et al*., 2010; *Sommer et al*., 2013a]. An algorithm was used to extract the T and S properties of 9401 interfaces and adjacent mixed layers

Table 1. Notation and Definitions

Parameter	Unit	Description	Calculation Method/Values Used: Kivu	Calculation Method/Values Used: DNS
		Density Related Parameters		
α	K^{-1}	thermal expansion coefficient	$(243 \text{ to } 278) \times 10^{-6}$	not needed
β	$kg\,g^{-1}$	haline contraction coefficient	$(0.89 \text{ to } 1.02) \times 10^{-3}$ (includes contribution of dissolved gases)	not needed
ρ_0	$kg\,m^{-3}$	reference density	1000 (mean density below 100 m depth)	997
T	$kg\,m^{-3}$	density contribution of temperature	$-\rho_0\alpha$ times in situ temperature (K)	direct
S	$kg\,m^{-3}$	density contribution of salt (and dissolved gases for Lake Kivu)	$\rho_0\beta$ times in situ salinity ($g\,kg^{-1}$)	direct
ρ	$kg\,m^{-3}$	density	$\rho_0 + T + S$	as Kivu
c_p	$J\,kg^{-1}\,K^{-1}$	specific heat capacity of water	4168 to 4177	4170
		Dimensional Control Parameters		
ΔT, ΔS	$kg\,m^{-3}$	T and S step across interface (Figure 2c)	difference of the mean T and S in the central 50% of the mixed layers above and below an interface (Figure 1a)	$\Delta T = 12 \times 10^{-4}$ (equivalent to 5 mK) (Figure 1a); $\Delta S = R_\rho \Delta T$
κ_T, κ_S	$m^2\,s^{-1}$	molecular diffusivity of temperature and salt	1.40×10^{-7}, 1.43×10^{-9}	1.44×10^{-7}, 1.44×10^{-9}
ν	$m^2\,s^{-1}$	kinematic viscosity	$(8.8 \text{ to } 9.4) \times 10^{-7}$	9×10^{-7}
H	m	layer height	interface thickness + mean thickness of the two adjacent mixed layers (Figure 1b)	domain height, 0.33 (Figure 1b)
		Dimensionless Control Parameters		
R_ρ	-	density ratio $\Delta S/\Delta T$	Figure 1c	2, 3, 4, 5, 6 (Figure 1c)
Ra	-	Rayleigh number $g\Delta T H^3/(\rho_0 \nu \kappa_T)$	Figure 1d	3.3×10^6 (Figure 1d)
Pr	-	Prandtl number ν/κ_T	6.41	6.25
τ	-	diffusivity ratio κ_S/κ_T	0.01	0.01

from the temperature and conductivity profiles. The algorithm is based on criteria relating small-scale gradients to background gradients and requesting approximate linearity in the interface core. For a detailed description of the data set, the evaluation algorithm, the sensor specifications, the density calculation, and the method for including dissolved gases in salinity, we refer to *Schmid et al.* [2010] and *Sommer et al.* [2013b].

2.2. DNS

For the DNS we use the code by *Winters et al.* [2004] to simulate a two-dimensional (2-D) incompressible Boussinesq fluid assuming a linear equation of state (Table 1). Note that the DNS uses the molecular values of κ_T, κ_S, and ν of a heat-salt system, which, for computational reasons, is not always the case in DNS [*Yoshida and Nagashima*, 2003; *Simeonov and Stern*, 2008]. The domain size of the simulation is 66 cm (horizontal) × 33 cm (vertical). The grid spacing Δx (in both directions) and time step Δt are 0.32 mm and 0.025 s, respectively, for $R_\rho = 2$, 3 and 0.64 mm and 0.1 s for $R_\rho = 4$, 5, 6. The grid spacing holds $\Delta x L_B^{-1} < 1.2$ for all simulations with $L_B = (\nu \kappa_S^2 \varepsilon^{-1})^{1/4}$ being the Batchelor scale of salt and ε being the rate of dissipation of turbulent kinetic energy. In a grid convergence study for the most critical simulation at $R_\rho = 4$ with $\Delta x L_B^{-1} = 1.2$, we found that various $\Delta x = 0.64$, 0.73, and 0.83 mm result in the same vertical fluxes of heat and salt and we are thus confident that the grid spacing is sufficiently small. The time step was chosen to fulfill the condition $\nu \Delta t \Delta x^{-2} < 0.25$.

At simulation start, an interface with two adjacent mixed layers is constructed by horizontally uniform hyperbolic tangent profiles with initial interface thicknesses $h_T = h_S = 3$ cm. Periodic boundary conditions are used on all boundaries except that ΔT and ΔS are added/subtracted to T and S of fluid crossing the vertical boundaries to ensure continuity in the vertical (i.e., an infinite staircase is constructed). Random noise is added to the vertical velocity field to seed convective instabilities that develop near the interface [*Carpenter et al.*, 2012b]. For each of the five simulations, we evaluate a time interval of 13 h after a quasi steady state has been reached. Every 12.5 min, vertical T and S profiles are extracted from the simulated T/S field at horizontal intervals of 1 cm. Each profile is evaluated in the same way as the profiles measured in Lake Kivu.

2.3. Comparison

For the direct comparison of interface thicknesses and fluxes for DNS and Lake Kivu, we match the parameters ΔT, H, and R_ρ in both systems. This is done by sorting the Lake Kivu data into bins of ΔT, H, and R_ρ that

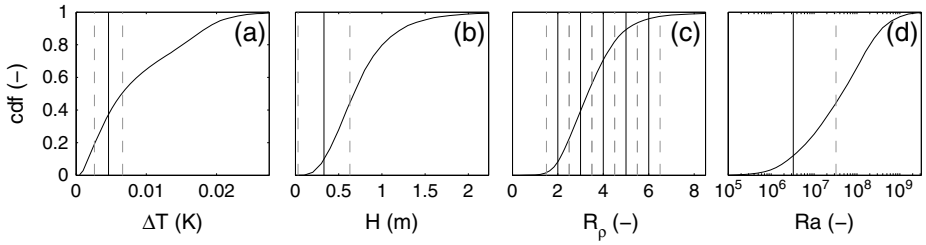

Figure 1. (a–d) Lake Kivu parameter distributions represented by cumulative distribution functions (cdf) and their subsets used for the comparison to the DNS. The bins of the Lake Kivu subsets, indicated by dashed vertical lines in Figures 1a–1c, are centered around the fixed DNS parameters (solid vertical lines). The dashed vertical line in Figure 1d indicates the largest *Ra* derived from the bins in Figures 1a and 1b. The smallest *Ra* = 1400 is outside the range of Figure 1d.

correspond to the approximately fixed values of the DNS (Figure 1). The values of R_ρ used in the five simulations span the range observed in Lake Kivu. Due to computational considerations, ΔT (corresponding to 5 mK) and H (0.33 m) are chosen a factor of ~2 smaller than the average values in Lake Kivu. For $R_\rho = (2, 3, 4, 5, 6)$, the Lake Kivu and DNS bins contain (297, 409, 260, 124, 66) and (4895, 4737, 11798, 18715, 20860) interfaces and mixed layers, respectively. The reason for the varying number of interfaces in the DNS bins is that only undisturbed interfaces, through which the vertical transport is purely molecular, are evaluated. As a consequence, (74, 77, 44, 13, 2)% of the interfaces in the DNS are rejected. For details on the rejection criterion we refer to *Sommer et al.* [2013b]. For Lake Kivu those percentages are (70, 61, 50, 33, 19), showing that for low R_ρ more interfaces are rejected than for large R_ρ. At large R_ρ, more interfaces are rejected for Lake Kivu than for the DNS because of electronic noise in the conductivity signal. The effects of rejecting such high percentages of interface measurements are examined later in the manuscript.

3. Results

3.1. Phenomenological Description of DNS and Lake Kivu Profiles

We begin with a qualitative description of the *T*/*S* structures observed in the DNS and relate these to vertical structures observed in the Lake Kivu staircase. In Figure 2 we show examples of the simulated density fields for $R_\rho \approx 2$ (at $t = 29$ h) and $R_\rho \approx 6$ (at $t = 61$ h). Below each density field, three profiles of T and S are shown (Figures 2c–2h) which are taken along the white vertical lines in Figures 2a and 2b. For each DNS profile a corresponding Lake Kivu profile example is presented (Figures 2i–2n).

For $R_\rho \approx 2$, S interfaces are either extremely thin ($h_S = 4$ mm and 2.3 mm in Figures 2d and 2j, respectively) or they contain very thin mixed regions (Figures 2e and 2k). Only interfaces that are undisturbed (Figures 2d and 2j) are analyzed, whereas the interfaces in Figures 2c, 2e, 2i, and 2k are discarded. The DNS suggests that mixed layer fluctuations are signals of distinct plumes (Figures 2c–2e) rather than homogeneous, isotropic turbulence acting on a background gradient. A plume usually consists of an *S*-dominated core (yellow color in the lower mixed layer in Figure 2a) driven by a *T*-dominated envelope (Figure 2d at $z \approx 25$ cm). Once the *T* envelope has vanished by diffusion, the *S* core tends to sink back toward the interface while it is advected by the mixed layer circulation (*S* signal in Figure 2c at $z \approx 26$ cm).

For $R_\rho \approx 6$, interfaces are thicker than for $R_\rho \approx 2$ and they are dominated by a diffusive core (green band in Figure 2b) which contains linear gradients in T and S. Plumes do not penetrate into the diffusive core, and plume signatures are barely visible in the mixed layers of the T and S profiles.

3.2. Comparison of Interface Thicknesses

We continue by comparing distributions and arithmetic means of interface thicknesses for the DNS and Lake Kivu, which are needed to calculate molecular fluxes through interfaces. The interface thickness of T (and analogously for S) is defined by

$$h_T = \left|\Delta T (\mathrm{d}T/\mathrm{d}z)^{-1}\right| \quad (1)$$

where $\mathrm{d}T/\mathrm{d}z$ is the vertical T gradient based on a linear fit in the central 50% of the interface. Two corrections are applied to h_T of the Lake Kivu measurements to account for the sensor responses and for underestimating the maximum gradient by the linear fit [*Sommer et al.*, 2013b]. The second correction is also applied for the DNS profiles.

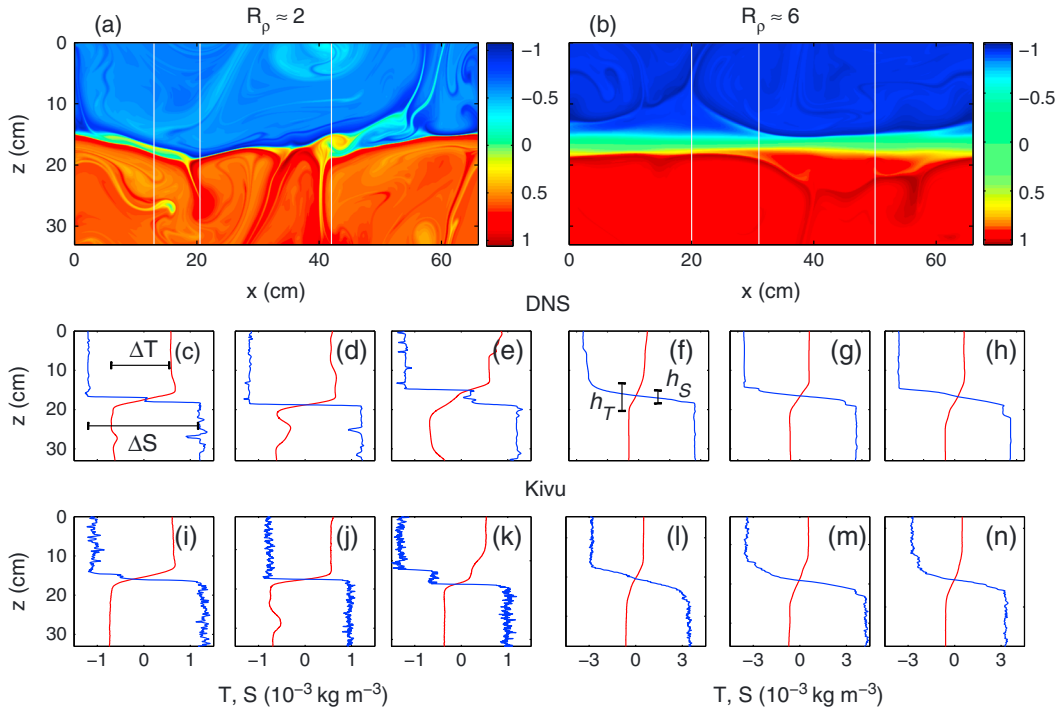

Figure 2. (a–n) Comparison of DNS and Lake Kivu interfaces and mixed layers for $R_\rho \approx 2$ and $R_\rho \approx 6$. The colors in Figures 2a and 2b (note the different scales) represent the density field (normalized with respect to the mean density and the maximum density difference), and the vertical lines indicate the positions of the T (red) and S (blue) profiles shown in Figures 2c–2h in the same order. Examples of matching Lake Kivu interfaces are shown in Figures 2i to 2n, and their positions [Latitude (°S), longitude (°E), depth (m)] are [2.03398, 29.19555, 336.91], [1.78898, 29.17548, 175.38], [1.78307, 29.18428, 201.50], [1.81588, 29.23947, 197.72], [1.91337, 29.22598, 184.50], [2.06203, 29.19227, 199.94], respectively.

Distributions of h_T and h_S (Figures 3a and 3b) for $R_\rho \approx 3$ are in excellent agreement between DNS and Lake Kivu, and the bimodal distribution of h_S is successfully reproduced by the DNS. The $R_\rho \approx 3$ regime can be understood qualitatively as an intermediate regime between small and large R_ρ and the double peak thus as a combination of the interface thicknesses shown in Figure 2. Extremely thin interfaces are seen in Figures 2d and 2j forming the left peak, whereas interfaces of intermediate thickness are often disturbed as in Figures 2e and 2k. Such interfaces are rejected by the algorithm and are thus missing in Figures 3a and 3b, creating the gap between the two peaks. Thick interfaces are as in Figures 2f–2h and 2l–2n and form the right peak. For $R_\rho \approx 3$, however, such thick interfaces are only found in profiles taken close to or within plumes.

The arithmetic means of h_T in the DNS and Lake Kivu (Figure 3c) agree well within the confidence intervals of the Lake Kivu estimates, except at $R_\rho = 2$, where the 2-D limitation of the DNS is thought to be important [*Flanagan et al.*, 2013]. The means of h_S are almost identical at $R_\rho = 3$, but at $R_\rho = 2$ the 2-D limitation might again cause the observed discrepancy. At large R_ρ, h_S in Lake Kivu is ~20% larger than in the DNS, which is partly caused by the choice of the bin sizes for the Lake Kivu data set.

In Figure 3d we decreased the binning intervals of ΔT and H by factors of 2 and 3, respectively, with Ra now ranging between 8.7×10^5 and 8.8×10^6. This results in a reduction of the Lake Kivu data set by factors of 4 to 6 and thus larger confidence intervals in Figure 3d. For all R_ρ except $R_\rho = 2$, $<h_T>$ and $<h_S>$ slightly decrease (maximum decrease by 14% at $R_\rho = 4$), and we expect that this is because the (on average) larger Rayleigh number corresponds to more vigorous convection in the mixed layer, larger fluxes, a more efficient erosion and thus thinning of the interface.

3.3. Comparison of Heat and Salt Fluxes and Density Flux Ratios

We use the interface thicknesses of the previous section to calculate molecular fluxes through interfaces, which we then compare to the total vertical fluxes in the DNS and to the flux parameterization by *Kelley* [1990] as well as to two theoretical predictions. The three different methods used to calculate heat fluxes F_H (W m^{-2}),

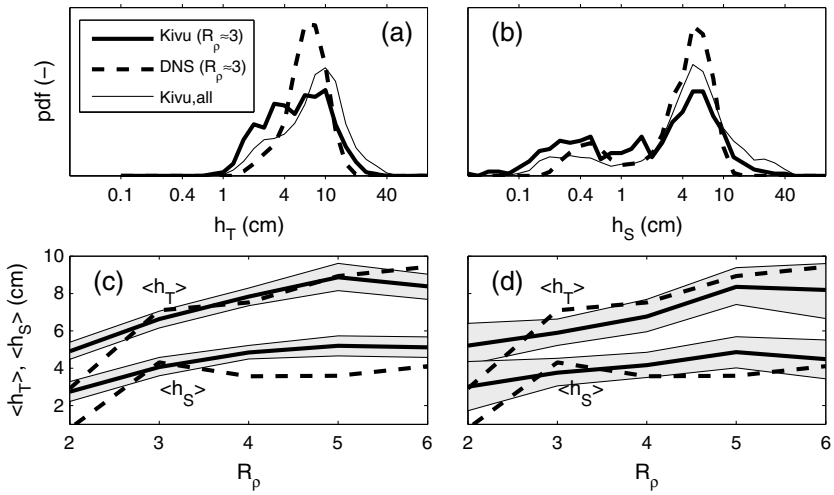

Figure 3. Comparison of T and S interface thicknesses for DNS and Lake Kivu observations. (a, b) The probability density functions (pdf) labeled "Kivu ($R_\rho \approx 3$)" ($n = 409$) and "DNS ($R_\rho \approx 3$)" ($n = 4734$) correspond to the subdata set with $R_\rho \approx 3$. For completeness, the entire Kivu data set (labeled "Kivu,all," $n = 9{,}401$) is shown. Note the logarithmic scales in Figures 3a and 3b. (c) Arithmetic means of h_T and h_S as a function of R_ρ with shadings representing bootstrapped 95% confidence intervals of the Lake Kivu data set. For DNS, the confidence intervals are thinner and close to the width of the dashed lines (not shown). (d) We reproduce Figure 3c but use a tighter binning for the Lake Kivu data set, as discussed in the text.

S fluxes F_S (in density units of kg m^{-2} s^{-1}), and density flux ratios $R_F = (c_p F_S)/(\alpha F_H)$ (-) are introduced in the following:

1. Molecular flux through the interface measured by a profile at a specific horizontal location: By definition of h_T and h_S

$$F_{H,\mathrm{mol}} = \frac{c_p}{\alpha}\kappa_T \frac{\Delta T}{h_T} \quad \left(\mathrm{W\ m^{-2}}\right) \tag{2a}$$

$$F_{S,\mathrm{mol}} = \kappa_S \frac{\Delta S}{h_S} \quad \left(\mathrm{kg\ m^{-2} s^{-1}}\right) \tag{2b}$$

2. Total vertical fluxes (only applicable for the DNS) estimated from the molecular transport across the central isotherm σ (located within the interface and assumed to be a material surface that moves with the fluid and is not affected by diffusion) (for details see *Winters and D'Asaro* [1996], *Carpenter et al.* [2012a], and *Carpenter and Timmermans* [2014])

$$F_{H,\mathrm{tot}} = \frac{c_p}{\alpha A}\int_\sigma \kappa_T |\nabla T| \mathrm{d}\sigma \quad \left(\mathrm{W\ m^{-2}}\right) \tag{3}$$

where A is the plane cross-sectional area (definition of $F_{S,\mathrm{tot}}$ analogously). If σ is a flat isotherm, then $F_{H,\mathrm{tot}}$ is identical to horizontally averaged estimates of $F_{H,\mathrm{mol}}$. For $R_\rho \approx 2$ and in particular for S, interfacial fluid was entrained into the mixed layers forming additional isothermal "islands" in the mixed layers. In that case $F_{H,\mathrm{tot}}$ was calculated by the sum of the integrals. We compared $F_{H,\mathrm{tot}}$ to another method of calculating the total flux given by $F_{H,\mathrm{adv}} = -c_p/\alpha <wT>_A$ where w is the vertical velocity and $<\cdot>$ indicates a spatial average over a plane area, A, that is taken in the center of the mixed layer. Both methods agree within 2% and 13% for T and S, respectively. The agreement confirms that equation (3) captures the total flux. In the following, we use $F_{H,\mathrm{tot}}$ because it exhibits less time variability and hence less dependence on the averaging period.

3. Fluxes calculated using the parameterization of *Kelley* [1990], based on laboratory data, dimensional analysis and assuming that F_H is independent of H

$$F_{H,\mathrm{Kel90}} = 0.0032 \exp\left(\frac{4.8}{R_\rho^{0.72}}\right) c_p \rho_0 \left(\frac{\kappa_T^2 g \alpha}{\nu}\right)^{1/3} \left(\frac{\Delta T}{\rho_0 \alpha}\right)^{4/3} \quad \left(\mathrm{W\ m^{-2}}\right) \tag{4a}$$

$$R_{F,\mathrm{Kel90}}(R_\rho) = \frac{R_\rho + 1.4(R_\rho - 1)^{3/2}}{1 + 14(R_\rho - 1)^{3/2}} \quad (-) \tag{4b}$$

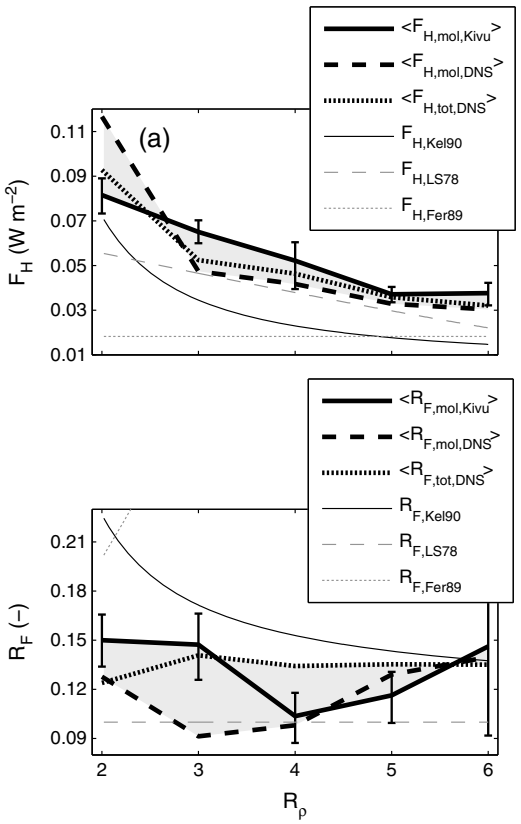

Figure 4. Comparison of (a) heat fluxes F_H and (b) density flux ratios R_F for DNS, Lake Kivu observations, and the parameterizations by *Kelley* [1990], *Linden and Shirtcliffe* [1978], and *Fernando* [1989b]. Vertical bars are bootstrapped 95% confidence intervals of $<F_{H,mol,Kivu}>$. For $<F_{H,mol,DNS}>$ and $<F_{H,tot,DNS}>$ the confidence intervals are within the width of the lines. The grey shadings visually group the Kivu and the DNS estimates.

Because ΔT is constant in the DNS equations (4a) and (4b) are only functions of R_ρ.

To compare the flux estimates of the DNS and Lake Kivu, we average spatially and temporally over the measurements from DNS and take ensemble averages from the corresponding Lake Kivu data bin (Figures 4a and 4b). Averages are indicated by angle brackets. We find that $<F_{H,mol,DNS}>$ underestimates $<F_{H,tot,DNS}>$ by less than 10% for $R_\rho \geq 3$, in agreement with the three-dimensional (3-D) simulations of *Carpenter et al.* [2012a]. This means that for $R_\rho \geq 3$, the total fluxes are well represented by molecular fluxes through the interfaces. For $R_\rho < 3$, $<F_{H,mol,DNS}>$ strongly depends on the rejection criterion for disturbed interfaces, which can lead to overestimates (as here, by 29%) as well as underestimates (without rejecting, 20%) of $<F_{H,tot,DNS}>$. We note that *Flanagan et al.* [2013] showed that at $R_\rho = 2$, 2-D simulations result in a factor of 1.5 smaller heat fluxes than the corresponding 3-D simulation. This questions, in general, the validity of the 2-D DNS in accurately capturing fluxes at small R_ρ. For $R_\rho \geq 3$, however, 3-D fluxes were found to agree well with the 2-D simulations. Comparing Lake Kivu and DNS heat fluxes, we find that $<F_{H,mol,Kivu}>$ agrees within 24% and 38% with $<F_{H,tot,DNS}>$ and $<F_{H,mol,DNS}>$, respectively, for the entire range of R_ρ.

The *Kelley* [1990] parameterization can be seen to underestimate $<F_{H,tot,DNS}>$ by a factor of 1.3 to 2.2. *Sommer et al.* [2013a] suggest a correction factor for the *Kelley* [1990] estimates based on a different choice of the exponent in the scaling of Nusselt number *Nu* to *Ra*, where *Nu* is F_H divided by the diffusive heat flux $c_p\kappa_T\Delta T/(\alpha H)$ (W m^{-2}). The suggested correction factor is ~1.6 and thus compensates for most of the observed difference and supports the scaling suggested by *Sommer et al.* [2013a].

The density flux ratio R_F agrees well between all estimates for large R_ρ and approaches $R_F = 0.15$ at $R_\rho \approx 6$, which is the constant value found in the first double-diffusion experiments by *Turner* [1965] for $2 < R_\rho < 7$. At small R_ρ, however, estimates from equations (2a), (2b), (3) and (4b) deviate from each other and do not follow the increase of $R_{F,Kel90}$ usually explained by increasingly turbulent interfaces. This discrepancy could have several reasons. (i) Laboratory measurements of R_F [*Kelley*, 1990, Figure 2] show an extremely sharp transition between approximately constant R_F at large R_ρ and the rapid increase for $1 < R_\rho < 2$. This transition is not captured accurately by the fit function used by *Kelley* [1990], and as a result, $R_{F,Kel90}$ overestimates laboratory data (as well as our measurements) by ~25% at $R_\rho \approx 2$. (ii) The 2-D limitation of the DNS questions the value of $<R_{F,tot,DNS}>$ at $R_\rho = 2$. (iii) The increasing portion of "turbulent" transport across the interface, in particular of *S*, is not accurately captured by computing $<R_{F,mol,Kivu}>$ and $<R_{F,mol,DNS}>$. Note, however, that rejecting disturbed interfaces is important, because without rejecting, $<R_{F,mol,Kivu}>$ and $<R_{F,mol,DNS}>$ would additionally decrease by a factor of ~2 at $R_\rho = 2$ and thus deviate substantially from both $<R_{F,tot,DNS}>$ and $R_{F,Kel90}$.

Reducing the bin size as in section 3.2 causes only small variations in $<F_{H,mol,Kivu}>$ and $<R_{F,mol,Kivu}>$ by less than 5% and 16%, respectively, and has thus only marginal effects on the qualitative comparison to the DNS estimates.

For completeness we also show two theoretical predictions for the heat flux and flux ratio in Figure 4. The theory of *Linden and Shirtcliffe* [1978] (their equations (2.21) and (2.9) for $F_{H,LS78}$ and $R_{F,LS78}$, respectively) is

based on the periodic formation of unstable boundary layers above and below the interface and their subsequent release into the mixed layers. In the theory of *Fernando* [1989a, 1989b] (equations (10b) and (12) for $F_{H,Fer89}$ and $R_{F,Fer89}$, respectively, in *Fernando* [1989b]) convective turbulence continuously erodes the interface and transports interfacial fluid into the mixed layers. Whereas the theory of *Fernando* [1989b] does not reproduce our measurements, the heat flux estimate of *Linden and Shirtcliffe* [1978] agrees within 32% to $<F_{H,tot,DNS}>$ for $R_\rho \geq 3$, which is better than $<F_{H,Kel90}>$ without the correction of *Sommer et al.* [2013a]. This suggests that at low $Ra = 3.3 \times 10^6$ (compared to $Ra = O(10^8)$ typical for laboratory experiments and average Ra in Lake Kivu) and for $R_\rho \geq 3$, double diffusion is rather controlled by the interfacial boundary layers than by mixed layer convection. However, a periodic release of interfacial boundary layer fluid as suggested by the model of *Linden and Shirtcliffe* [1978] is not directly observed in the DNS (Figure 2), except at simulation start after the initial diffusion of the *T* and *S* interfaces.

4. Conclusions

The diffusive type of double diffusion was studied by comparing direct numerical simulations (DNS) to microstructure profiles from Lake Kivu. We showed that two-dimensional DNS is a valuable tool for interpreting microstructure signals measured in natural environments and that the interface thickness distributions measured in Lake Kivu are successfully reproduced by DNS. For the DNS, we found that molecular heat fluxes through interfaces capture the total fluxes for $R_\rho \geq 3$ within 10% and that the DNS heat flux estimates agree well with the measured Lake Kivu estimates. This suggests that in Lake Kivu, double diffusion is the main contributor to the vertical "diffusive" flux, and external turbulence by shear or internal wave breaking is of minor effect. For both the DNS and Lake Kivu, heat fluxes were found larger than predicted by the parameterization of *Kelley* [1990]. Applying the correction factor suggested by *Sommer et al.* [2013a], which accounts for a different exponent in the Rayleigh/Nusselt number scaling, compensates for most of the difference.

The results are promising and motivate further comparison studies including a quantitative analysis of the mixed layer structure for variable Rayleigh numbers and domain sizes. Such studies might answer the question of whether turbulent flux methods [*Osborn and Cox*, 1972; *Osborn*, 1980] can be used as independent estimates for vertical fluxes in addition to molecular fluxes through interfaces and flux parameterizations.

Acknowledgments

We would like to thank Kraig Winters for providing the DNS code and Brian Dobbins for computational support. We also thank Natacha and Tom Tofield Pasche for their hospitality and organizational support in Rwanda as well as Fidèle Kanamugire, owner of the transportation vessel "Gloria", his crew, and Michael Schurter for their excellent work on the lake. Martin Schmid provided valuable comments on an earlier version of the manuscript. We kindly provide the data used in this work on request to the reader. The project was supported by the Swiss National Science Foundation under grants 200021-122183 and 200020-140538 (Lake Kivu—turbulence and double diffusion in permanent stratification) and in part by the Yale University Faculty of Arts and Sciences High Performance Computing facility (and staff).

The Editor thanks two anonymous reviewers for their assistance in evaluating this paper.

References

Carpenter, J. R., T. Sommer, and A. Wüest (2012a), Simulations of a double-diffusive interface in the diffusive convection regime, *J. Fluid Mech.*, *711*, 411–436, doi:10.1017/jfm.2012.399.

Carpenter, J. R., T. Sommer, and A. Wüest (2012b), Stability of a double-diffusive interface in the diffusive convection regime, *J. Phys. Oceanogr.*, *42*(5), 840–854, doi:10.1175/JPO-D-11-0118.1.

Carpenter, J. R., and M.-L. Timmermans (2014), Does rotation influence double-diffusive fluxes in polar oceans?, *J. Phys. Oceanogr.*, *44*(1), 289–296, doi:10.1175/JPO-D-13-098.1.

Descy, J.-P., F. Darchambeau, and M. Schmid (Eds.) (2012), *Lake Kivu: Limnology and Biogeochemistry of a Tropical Great Lake*, *Aquat. Ecol. Ser.*, vol. 5, Springer, Dordrecht, Heidelberg, New York, and London.

Fernando, H. J. S. (1989a), Buoyancy transfer across a diffusive interface, *J. Fluid Mech.*, *209*, 1–34, doi:10.1017/S0022112089003010.

Fernando, H. J. S. (1989b), Oceanographic implications of laboratory experiments on diffusive interfaces, *J. Phys. Oceanogr.*, *19*(11), 1707–1715, doi:10.1175/1520-0485(1989)019<1707:OIOLEO>2.0.CO;2.

Flanagan, J. D., A. S. Lefler, and T. Radko (2013), Heat transport through diffusive interfaces, *Geophys. Res. Lett.*, *40*, 2466–2470, doi:10.1002/grl.50440.

Gregg, M. C., and T. B. Sanford (1987), Shear and turbulence in thermohaline staircases, *Deep Sea Res. Part A*, *34*(10), 1689–1696, doi:10.1016/0198-0149(87)90017-3.

Kelley, D. E. (1990), Fluxes through diffusive staircases: A new formulation, *J. Geophys. Res.*, *95*(C3), 3365–3371, doi:10.1029/JC095iC03p03365.

Kelley, D. E., H. J. S. Fernando, A. E. Gargett, J. Tanny, and E. Özsoy (2003), The diffusive regime of double-diffusive convection, *Prog. Oceanogr.*, *56*(3–4), 461–481, doi:10.1016/S0079-6611(03)00026-0.

Kimura, S., and W. Smyth (2007), Direct numerical simulation of salt sheets and turbulence in a double-diffusive shear layer, *Geophys. Res. Lett.*, *34*, L21610, doi:10.1029/2007GL031935.

Linden, P. F., and T. G. L. Shirtcliffe (1978), The diffusive interface in double-diffusive convection, *J. Fluid Mech.*, *87*(03), 417–432, doi:10.1017/S002211207800169X.

Newman, F. C. (1976), Temperature steps in Lake Kivu: A bottom heated saline lake, *J. Phys. Oceanogr.*, *6*(2), 157–163, doi:10.1175/1520-0485(1976)006<0157:TSILKA>2.0.CO;2.

Noguchi, T., and H. Niino (2010a), Multi-layered diffusive convection. Part 1. Spontaneous layer formation, *J. Fluid Mech.*, *651*, 443–464, doi:10.1017/S0022112009994150.

Noguchi, T., and H. Niino (2010b), Multi-layered diffusive convection. Part 2. Dynamics of layer evolution, *J. Fluid Mech.*, *651*, 465–481, doi:10.1017/S0022112010994160.

Osborn, T. R. (1980), Estimates of the local rate of vertical diffusion from dissipation measurements, *J. Phys. Oceanogr.*, *10*(1), 83–89, doi:10.1175/1520-0485(1980)010<0083:EOTLRO>2.0.CO;2.

Osborn, T. R., and C. S. Cox (1972), Oceanic fine structure, *Geophys. Fluid Dyn.*, *3*(1), 321–345, doi:10.1080/03091927208236085.

Ruddick, B., and A. E. Gargett (2003), Oceanic double-infusion: Introduction, *Prog. Oceanogr.*, *56*(3–4), 381–393, doi:10.1016/S0079-6611(03)00024-7.

Schmid, M., M. Busbridge, and A. Wüest (2010), Double-diffusive convection in Lake Kivu, *Limnol. Oceanogr.*, *55*(1), 225–238.
Schmitt, R. W. (1994), Double diffusion in oceanography, *Annu. Rev. Fluid Mech.*, *26*(1), 255–285, doi:10.1146/annurev.fl.26.010194.001351.
Simeonov, J., and M. E. Stern (2008), Double-diffusive intrusions in a stable salinity gradient "heated from below", *J. Phys. Oceanogr.*, *38*(10), 2271–2282, doi:10.1175/2008JPO3913.1.
Sommer, T., J. R. Carpenter, M. Schmid, R. G. Lueck, M. Schurter, and A. Wüest (2013a), Interface structure and flux laws in a natural double-diffusive layering, *J. Geophys. Res. Ocean.*, *118*(11), 6092–6106, doi:10.1002/2013JC009166.
Sommer, T., J. R. Carpenter, M. Schmid, R. G. Lueck, and A. Wüest (2013b), Revisiting microstructure sensor responses with implications for double-diffusive fluxes, *J. Atmos. Oceanic Technol.*, *30*(8), 1907–1923, doi:10.1175/JTECH-D-12-00272.1.
Timmermans, M.-L., J. Toole, R. Krishfield, and P. Winsor (2008), Ice-tethered profiler observations of the double-diffusive staircase in the Canada Basin thermocline, *J. Geophys. Res.*, *113*, C00A02, doi:10.1029/2008JC004829.
Traxler, A., S. Stellmach, P. Garaud, T. Radko, and N. Brummel (2011), Dynamics of fingering convection. Part 1 Small-scale fluxes and large-scale instabilities, *J. Fluid Mech.*, *677*, 530–553, doi:10.1017/jfm.2011.98.
Turner, J. S. (1965), The coupled turbulent transports of salt and heat across a sharp density interface, *Int. J. Heat Mass Transfer*, *8*(5), 759–767, doi:10.1016/0017-9310(65)90022-0.
Turner, J. S. (2010), The melting of ice in the Arctic Ocean: The influence of double-diffusive transport of heat from below, *J. Phys. Oceanogr.*, *40*(1), 249–256, doi:10.1175/2009JPO4279.1.
Winters, K. B., and E. A. D'Asaro (1996), Diascalar flux and the rate of fluid mixing, *J. Fluid Mech.*, *317*, 179–193, doi:10.1017/S0022112096000717.
Winters, K. B., J. A. MacKinnon, and B. Mills (2004), A spectral model for process studies of rotating, density-stratified flows, *J. Atmos. Oceanic Technol.*, *21*(1), 69–94, doi:10.1175/1520-0426(2004)021<0069:ASMFPS>2.0.CO;2.
Yoshida, J., and H. Nagashima (2003), Numerical experiments on salt-finger convection, *Prog. Oceanogr.*, *56*(3–4), 435–459, doi:10.1016/S0079-6611(03)00032-6.